Torque Ripple Suppression Method based on FOC for SRM without FEM analysis

Kouki Tokui, Takahiro Kumagai, Jun-ichi Itoh
Nagaoka University of Technology
1603-1 Kamitomioka-machi, Nagaoka city, Niigata, Japan
Tel., Fax: +81 / (258) – 47.9533.
E-Mail: s183148@stn.nagaokaut.ac.jp, itoh@vos.nagaokaut.ac.jp
URL: http://itohserver01.nagaokaut.ac.jp/itohlab/en/index.html

Keywords

«Switched reluctance drive», «Third harmonic injection», «Vibration suppression», «Vector control»

Abstract

This paper proposes a torque ripple suppression method for a switched reluctance motor (SRM) with only measurable parameters. A large third-order torque ripple is generated by a conventional method with constant *dq*0-axis current, which is *dq*-axis current and zero-phase current converted from the three phase current of SRM. Moreover, the conventional method assumes an inductance profile constant regarding a change in the current. In the magnetic saturation region, the inductance decreases at an aligned position. Thus, an effect of the torque ripple suppression method becomes low and the average torque cannot be controlled in the magnetic saturation region. The proposed method derives the zero-phase current with the third-order harmonic in order to suppress the torque ripple from a torque equation considering spatial harmonics of the inductance profile up to the forth order and torque/current ratio in whole region. In addition, an average torque control is proposed for the magnetic saturation region. The average torque equation is derived from the inductance expressing the magnetic co-energy at the magnetic saturation. As a result, the experiments demonstrated that the torque ripple is reduced by 76.1% in the linear region and by 73.4% in the magnetic saturation region compared to the conventional method with the constant *dq*0-axis current. Moreover, the derived average torque equation agrees with the experimental results including the error of 3.9%.

Introduction

A switched reluctance motor (SRM) has an advantage of low cost because SRM consists only of a plunger core and concentrated windings without magnets. In addition, SRM is suitable for high speed rotation and high temperature environment because the rotor of SRM is built with a solid salient pole core structure. Therefore, SRM is expected to be used in various applications such as home appliances, industry, and automobiles [1]-[4]. SRM rotates continuously by switching the single-phase excitation mode [5]. In general, the single-phase current is decided by the requirement torque. However, the single-pulse current causes a large torque ripple because the torque of SRM is decreased by the switching timing of the excitation phase. Moreover, the vibration of the stator becomes large because the radial force on the stator changes steeply.

References [6]-[9] have proposed the reduction method of the torque ripple and the radial force ripple. These methods use a torque-current-angle (T-i-θ_e) characteristic and a radial force-current-angle (F_r-i-θ_e) characteristic. Finite Element Method (FEM) analysis is usually used to obtain the T-i-θ_e characteristic and the F_r-i-θ_e characteristic because the measurement of these characteristics requires many procedures in the experiment due to necessity for many measurement points. However, the FEM analysis requires the exact geometric dimensions and the material property (B-H characteristic) of the motor. The users do not always have the exact geometric dimension and the material property. In addition, the result of the FEM analysis separates the result measured from the actual motor by the effect of the flux leakage at the coil ends [10]. Therefore, it is required to suppress the torque ripple and the radial force ripple by using only parameters that are easy measured by the experiment. Moreover, the

hysteresis current control is generally used to drive SRM. However, since the switching frequency of the hysteresis control is variable, the acoustic noise increases when the switching frequency matches the natural frequency of the mechanical system. In addition, the very high switching frequency is required in order for the noise to avoid the audible range (< 20 kHz) since the ratio of the inductance at the aligned position to the inductance at the unaligned position changes from 6 to 10.

The adjustable speed drive with the sinusoidal current for each phase has been proposed in order to reduce the noise and the vibration of SRM because the sinusoidal current changes smoothly compared to the single-pulse current [11]. In particular, references [12] and [13] has proposed Field Oriented Control (FOC, i.e. vector control) for SRM. The controller of FOC is designed only with the basic motor parameters such as the self-inductance and the winding resistance. The three-phase current of SRM is converted to the rotating frame (*dq*-axis) current and the zero-phase current by using the coordinate transformation in FOC. However, it seems that there are two problems; (i) the third-order torque ripple occurs in the rotor of SRM when the *dq*0-axis current are controlled to a constant value in the liner region. (ii) The effect of the magnetic saturation is ignored.

This paper proposes a torque ripple suppression method for the third-order torque ripple in whole flux region which includes the magnetic saturation. The proposed method derives the zero-phase current with the third-order harmonics in order to suppress the torque ripple from the torque equation and torque/current ratio in the whole flux region. In addition, the accurate average torque control is proposed in the magnetic saturation region. The average torque equation is derived from the inductance expressing the magnetic co-energy at the magnetic saturation. These proposed methods use the flux linkage at the aligned position and the inductance profile in the linear region, which are obtained without the FEM analysis because these methods use only parameters that are easy measured by the experiment.

This paper is organized as follows: firstly, the torque ripple suppression method in the linear region is described. Secondly, the torque ripple suppression method and the average torque control in magnetic saturation region is described. Finally, the torque ripple of the proposed method is evaluated by the experiment compared to that of the conventional method.

Toque Ripple Suppression Method in Linear Region

In this chapter, the torque ripple suppression method in the linear region is proposed.

Fig .1 shows the inductance profile which mentions the character between the self-inductance and the electrical angle. The inductance profile in Fig .1 is expressed as (1),

$$L_x = L_{dc} + \sum_{N=1}^{4} L_{acN} \cos\left(N\theta_e - \frac{2\pi}{3} x \right) \qquad (1)$$

where L_x is the self-inductance of each phase, x=0, 1, 2 indicates the u-, v-, w-phase, respectively. L_{dc} is the dc component of the self-inductance, L_{acN} is the N-th harmonic component of the self-inductance, θ_e is the electrical angle which is zero when the rotor is at the aligned position. The instantaneous torque equation of SRM is expressed as (2) and the coordinate transformation matrix is expressed as (3),

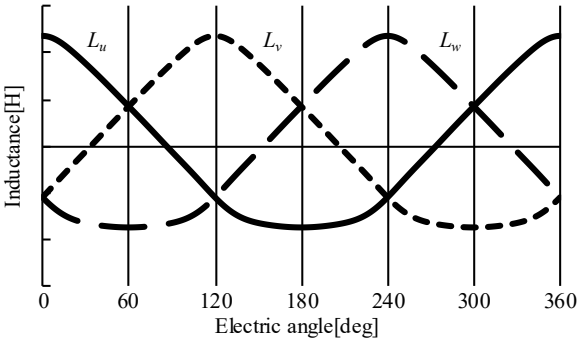

Fig. 1. Inductance profile including the spatial harmonics

$$T_e = \frac{N_r}{2} \begin{bmatrix} i_u & i_v & i_w \end{bmatrix} \left(\frac{\partial}{\partial \theta_e} \begin{bmatrix} L_u & 0 & 0 \\ 0 & L_v & 0 \\ 0 & 0 & L_w \end{bmatrix} \right) \begin{bmatrix} i_u \\ i_v \\ i_w \end{bmatrix} \qquad (2)$$

$$\begin{bmatrix} i_d \\ i_q \\ i_0 \end{bmatrix} = \frac{2}{3} \begin{bmatrix} \cos\theta_e & \cos\left(\theta_e - \frac{2}{3}\pi\right) & \cos\left(\theta_e + \frac{2}{3}\pi\right) \\ -\sin\theta_e & -\sin\left(\theta_e - \frac{2}{3}\pi\right) & -\sin\left(\theta_e + \frac{2}{3}\pi\right) \\ \frac{1}{2} & \frac{1}{2} & \frac{1}{2} \end{bmatrix} \begin{bmatrix} i_u \\ i_v \\ i_w \end{bmatrix} \qquad (3)$$

where N_r is a number of the rotor poles, i_u, i_v, i_w are the current of each phase, i_d is the d-axis current, i_q is the q-axis current, i_0 is the zero-phase current. By transforming (2) with (3), the instantaneous torque equation is expressed as (4),

$$\begin{aligned} T_{e\_har} &= \frac{3}{2}N_r L_{ac1} i_0 i_q + \frac{3}{8}N_r L_{ac1}\left({i_q}^2 - {i_d}^2\right)\sin 3\theta_e - \frac{3}{4}N_r L_{ac1} i_d i_q \cos 3\theta_e + \frac{3}{2}N_r L_{ac2} i_q i_d \\ &- 3N_r L_{ac2} i_0\left(i_d \sin 3\theta_e + i_q \cos 3\theta_e\right) - \frac{9}{4}N_r L_{ac3}\left({i_d}^2 \sin 3\theta_e + {i_q}^2 \sin 3\theta_e + 2{i_0}^2 \sin 3\theta_e\right) \\ &- 6N_r L_{ac4} i_0 i_d \sin 3\theta_e + 6N_r L_{ac4} i_q i_0 \cos 3\theta_e + \frac{3}{2}N_r L_{ac4}({i_q}^2 - {i_d}^2)\sin 6\theta_e - 3N_r L_{ac4} i_q i_d \cos 6\theta_e \end{aligned} \tag{4}$$

From (4), the torque contains third-order and six-order ripple when $dq0$-axis current command is constant. This paper focuses on the third-order torque ripple, which is the main torque ripple. Based on (4), the zero-phase current command that cancels out the third-order torque ripple is derived. The zero-phase current with the superimposed third-order harmonics is defined as (5),

$$I_{0\_har} = I_0 + \left(-\frac{1}{4}I_q + I_{0\_3s}\right)\sin 3\theta_e + I_{0\_3c}\cos 3\theta_e \tag{5}$$

where I_q is the average q-axis current in one cycle of the electrical angle and I_0 is the average zero phase current in one cycle of the electrical angle, I_{0_3s} is the sine component of the third-order harmonic current, I_{0_3c} is the cosine component of the third-order harmonic current. I_{0_3s} and I_{0_3c} are set to cancel out the third-order torque ripple. By substituting (5) into (4), the third-order torque ripple is expressed as (6).

$$T_{ripple} = A\sin 3\theta_e + B\cos 3\theta_e \tag{6}$$

$$\begin{aligned} A &= \frac{3}{2}N_r L_{ac1} I_{0\_3s} I_q - \frac{315}{128}N_r L_{ac3}{I_q}^2 - \frac{9}{2}N_r L_{ac3}{I_0}^2 - \frac{9}{8}N_r L_{ac3}{I_{0\_3c}}^2 \\ &+ \frac{27}{16}N_r L_{ac3} I_{0\_3s} I_q - \frac{27}{8}N_r L_{ac3}{I_{0\_3s}}^2 \end{aligned} \tag{7}$$

$$\begin{aligned} B &= \frac{3}{2}N_r L_{ac1} I_{0\_3c} I_q - 3N_r L_{ac2} I_0 I_q + \frac{9}{32}N_r L_{ac3} I_q I_{0\_3c} \\ &- \frac{9}{8}N_r L_{ac3} I_{0\_3c} I_{0\_3s} + 6N_r L_{ac4} I_0 I_q \end{aligned} \tag{8}$$

I_{0_3s} and I_{0_3c} have to be derived on the condition that A=0 and B=0 in order to cancel the third-order torque ripple in (6). However, the condition equation in (7) and (8) is the forth order equation for I_{0_3s} and I_{0_3c}. Thus, the approximated values of I_{0_3s} and I_{0_3c} is derived ignoring the terms in (7) and (8) that have a small effect to the torque ripple in order to simplify implementation. This paper assumes three following conditions for the approximation; first, the current commands are $I_q = I_0$; second, each spatial harmonic component is smaller than the fundamental component; third, the amplitude of the superimposed harmonic components are smaller than I_q. In other words, (7) and (8) are approximated with $I_q = I_0$, $(L_{ac2}/L_{ac1}) < 1$, $(L_{ac3}/L_{ac1}) < 1$, $(L_{ac4}/L_{ac1}) < 1$, $(I_{0\_3c}/I_q) < 1$, and $(I_{0\_3s}/I_q) < 1$. Since the forth and sixth terms in (7) and the forth term in (8) is regarded as zero due to the approximation, the required third-order harmonic current are expressed as (9) and (10).

$$I_{0\_3s} = \frac{297L_{ac3}I_q}{64L_{ac1} + 72L_{ac3}} \tag{9}$$

$$I_{0\_3c} = \frac{16\left(L_{ac2} - 2L_{ac4}\right)I_q}{8L_{ac1} + 3L_{ac3}} \tag{10}$$

Substituting (9) and (10) into (5), the zero-phase current with the superimposed third-order harmonics is expressed as (11).

$$I_{0\_har} = I_0 + \left(-\frac{1}{4}I_q + \frac{297L_{ac3}I_q}{64L_{ac1} + 72L_{ac3}}\right)\sin 3\theta_e + \frac{16\left(L_{ac2} - 2L_{ac4}\right)I_q}{8L_{ac1} + 3L_{ac3}}\cos 3\theta_e \tag{11}$$

Toque Ripple Suppression Method in Magnetic Saturation Region

In the previous chapter, the torque ripple suppression method in (11) was proposed under the condition that the inductance profile is constant regardless the change in the current. However, the inductance at the aligned position decreases in the case of the magnetic saturation. As a result, the torque ripple remains even when the superimposed current in (11) is applied because the approximated torque ripple and the actual torque ripple are different. In addition, the average torque cannot be controlled due to the magnetic saturation. This chapter proposes the average torque control method and the torque ripple suppression method in the magnetic saturation region.

Average torque control method in magnetic saturation region

Fig. 2 shows the i-ϕ characteristic at the aligned position. As shown in Fig. 2, the aligned inductance is defined as (a) the average inductance L_{a_avg} and (b) the incremental inductance L_{a_inc}. Generally, the average inductance is used in the linear region. The aligned inductance L_{a_avg} is the maximum value and the unaligned inductance L_{un} is the minimum value in the inductance profile. Therefore, L_{ac1} is approximated as (12) when the inductance profile is assumed as the sinusoidal wave.

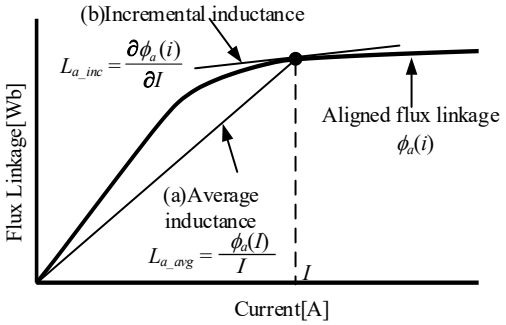

Fig. 2. Traditional definition of saturated inductance in SRM.

$$L_{ac1}=\frac{L_{a\_avg}-L_{un}}{2} \tag{12}$$

The first term of (4) expresses the average torque when i_q and i_0 is constant in one cycle of the electrical angle and i_d=0. Substituting (12) into the first term of (4), the conventional average torque equation is expressed as (13),

$$T_{avg\_conv.}=\frac{3}{2}N_r\frac{L_{a\_avg}-L_{un}}{2}I_qI_0 \tag{13}$$

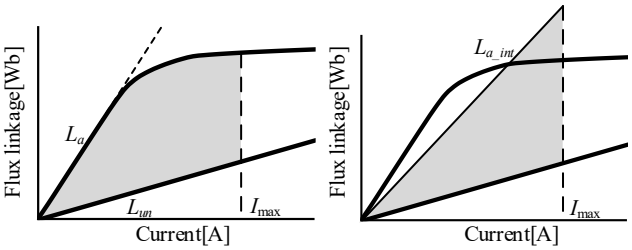

(a) Real (right side of (14)) (b) Assumption (left side of (14))

Fig. 3. Magnetic co-energy of maturated i-ϕ characteristic.

The inductance is almost not affected by the magnetic saturation at the unaligned position because the magnetic resistance of the air gap is large. On the other hand, the effect of the saturation is significant at the aligned position. Therefore, the aligned inductance is needed to correct in the magnetic saturation region.

The torque corresponds to the area of the i-ϕ characteristic in Fig. 2. However, the average inductance L_{a_avg} and the incremental inductance L_{a_inc} do not express the area of the i-ϕ characteristic. L_{a_avg} and L_{a_inc} are not appropriate as the inductance used in the average torque equation at the magnetic saturation.

Fig. 3 shows the i-ϕ characteristics at the unaligned position and the aligned position. The shaded area in Fig. 3(a) is the magnetic co-energy between the unaligned i-ϕ characteristic and the unaligned i-ϕ characteristic. This paper defines a novel inductance L_{a_int}, which equalizes the area of the shaded area in Fig. 3(a) and (b). Equation (14) expresses the equal area in Fig. 3(a) and (b),

$$\int_0^{I_{max}}(L_{a\_int}-L_{un})i\,di=\int_0^{I_{max}}\{\phi_a(i)-L_{un}i\}\,di \tag{14}$$

where I_{max} is the maximum current value and $\phi_a(i)$ is the aligned flux linkage. L_{a_int} is derived by substituting a polynomial approximation of $\phi_a(i)$ into (14). Substituting the derived L_{a_int} instead of L_{a_avg} in (13), the average torque equation in the magnetic saturation region is derived as (15),

$$T_{avg\_pro.}=\frac{3}{2}N_r\left(\sum_{n=1}^{N}k_n\frac{I_{max}^{\,n-1}}{n+1}-\frac{1}{2}L_{un}\right)I_qI_0 \tag{15}$$

where N is the approximation order of $\phi_a(i)$, k_n is the coefficient of the polynomial approximation. The average torque in the magnetic saturation region is calculated by (15).

Torque ripple suppression method in magnetic saturation region

Fig. 4 shows an example of the flux linkage and the torque waveforms when the magnetic saturation occurs. The magnetic saturation occurs when the rotor is near the aligned position and the current increases. As a result, the flux linkage becomes large as shown in Fig. 4. The output torque decreases because the ratio of the flux linkage to the current becomes low due to the magnetic saturation. On the other hand, the output torque in the linear region is higher than that in the saturation region because the flux linkage is proportional to the current. Thus, the torque ripple under the saturation region is caused by the alternating output of larger and smaller torque than the average torque.

Fig. 5 shows the i-ϕ characteristics when a small change of the current ΔI is given. As shown in Fig. 5(a), the red shaded area is the fine section of the i-ϕ characteristic in the saturation region. By dividing the fine section by the current I_{sat} in Fig. 5, the torque/current ratio in the saturation region is obtained. The torque/current ratio in the linear region and during average torque control is obtained in the same way. As a result, the torque/current ratio in each region is expressed as (16)-(18),

$$\frac{\Delta S_{lin}}{I_{lin}} = \frac{\left(\phi_{a\_lin} - \phi_{un\_lin}\right)\times\Delta I}{I_{lin}} = \left(L_{a\_lin} - L_{un}\right)\times\Delta I \tag{16}$$

$$\frac{\Delta S_{sat}}{I_{sat}} = \frac{\left(\phi_{a\_sat} - \phi_{un\_sat}\right)\times\Delta I}{I_{sat}} = \left(L_{a\_avg} - L_{un}\right)\times\Delta I \tag{17}$$

$$\frac{\Delta S_{avg}}{I_{avg}} = \frac{\left(\phi_{a\_avg} - \phi_{un\_sat}\right)\times\Delta I}{I_{avg}} = \left(L_{a\_\mathrm{int}} - L_{un}\right)\times\Delta I \tag{18}$$

where ΔS_{lin}, ΔS_{sat}, ΔS_{avg} are the fine sections of the i-ϕ characteristic in the linear region, in the saturation region, and for the average torque control, respectively. I_{lin}, I_{sat}, I_{avg} are the current in the linear region, in the saturation region, and for the average torque control, respectively. ϕ_{a_lin}, ϕ_{a_sat}, ϕ_{a_avg} are the magnetic flux linkage at the aligned position in the linear region, in the saturation region, and for the average torque control, respectively. ϕ_{un_lin}, ϕ_{un_sat}, ϕ_{un_avg} are the magnetic flux linkage at the unaligned position in the linear region, in the saturation region, and for the average torque control, respectively. L_{a_lin} is the linear inductance at the aligned position, L_{a_avg} is the average inductance at the aligned position. As mentioned previously, the torque ripple is caused by the difference of the torque/current ratio between the linear region and the saturation region. Thus, the torque ripple in the magnetic saturation region is expressed as (19) from (16)-(18).

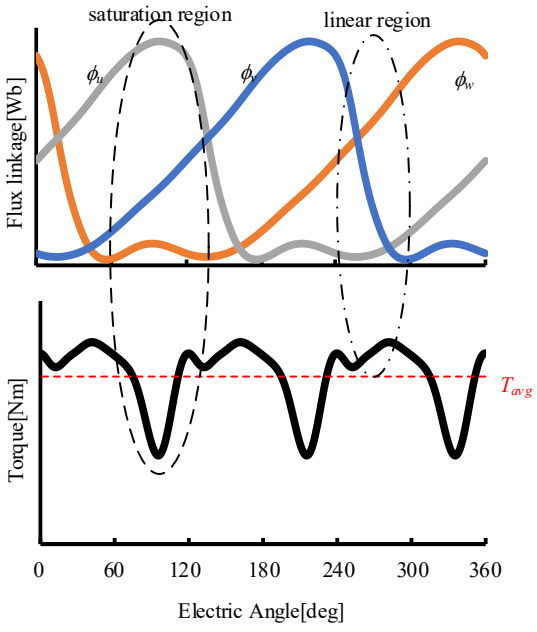

Fig. 4. Comparison of torque in the saturation and linear region.

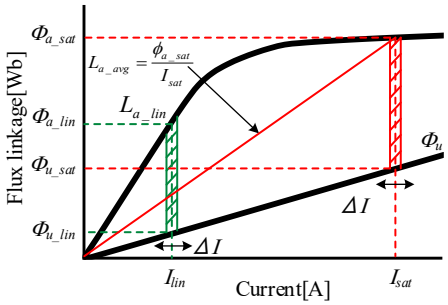

(a) Linear and saturation torque.

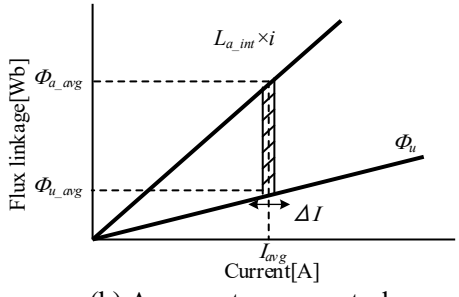

(b) Average torque control.

Fig. 5. Comparison of torque current ratio.

$$T_{rip} = T_{avg}\frac{S_{lin}/I_{lin}}{S_{avg}/I_{avg}} - T_{avg}\frac{S_{sat}/I_{sat}}{S_{avg}/I_{avg}} = T_{avg}\frac{L_{a\_lin}-L_{a\_avg}}{L_{a\_\mathrm{int}}-L_{un}} \tag{19}$$

The torque ripple is suppressed by increasing the current value in the saturation region, where the torque/current ratio is low, and by decreasing the current value in the linear region, where the torque/current ratio is high. Since the relationship between the average torque T_{avg} and the zero-phase current I_0 is expressed as (15), the superimposed zero-phase current in the magnetic saturation region is expressed as (20). Also, the zero-phase current command is expressed as (21),

$$I_{0\_sat} = \frac{L_{a\_avg}-L_{a\_lin}}{2\left(L_{a\_\mathrm{int}}-L_{un}\right)} I_0 \sin 3\left(\theta_e+\varphi\right) + \frac{L_{a\_lin}-L_{un}}{L_{a\_lin}+L_{a\_avg}-2L_u}\frac{L_{a\_lin}-L_{a\_avg}}{2\left(L_{a\_\mathrm{int}}-L_{un}\right)} I_0 \tag{20}$$

$$I_{0\_com} = I_{0\_har} + I_{0\_sat} \tag{21}$$

where φ is the phase where the magnetic flux linkage becomes the maximum value. The third-order current is superimposed on the zero-phase current in order to suppress the torque ripple, which occurs at three times the electrical frequency. The parameters shown in (20)-(21) requires only L_{a_avg}, L_{a_lin}, L_{a_int}, L_{un}, and the spatial harmonic of the inductance profile up to forth order, which are easy measured by the experiment and can eliminate the necessity of FEM.

Experimental Results

In this chapter, the effect of the torque ripple suppression in the linear region, the average torque control method, and the torque ripple suppression method in the magnetic saturation region are confirmed by the experiment. Fig. 6 shows the photograph of the experimental equipment, Table1 shows the motor parameter of SRM used in this experiment.

Fig. 7 shows the inductance profile obtained from the experiment and the FEM analysis. The spatial harmonics of the inductance profile up to the forth order are obtained by the harmonic analysis of Fig. 7. In the acquisition of the inductance profile in the linear region, the fixed test is not necessary because a small current is applied. The characteristics in Fig. 7 is obtained by applying the pulse voltage and acquiring the triangular current during the rotation operation [14].

Fig. 8 shows the i-ϕ characteristic at the aligned position and the unaligned position in the experiment

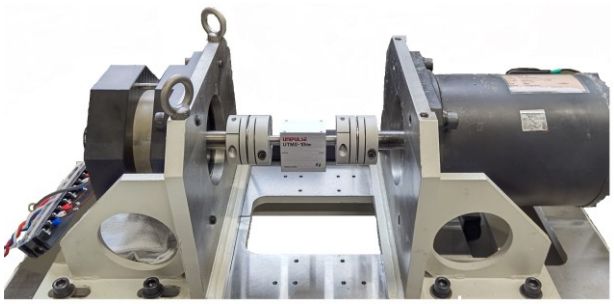

Fig. 6. Experimental equipment.

Table1. Motor parameters.

Rated power	2.2 kW
Maximum speed	7200 r/min
Maximum torque	4.38 Nm
Input voltage	300 V
Number of poles	Stator 18, Rotor 12
Winding resistance	0.45 Ω
Stator diameter	126 mm
Thickness of motor core	45.4 mm

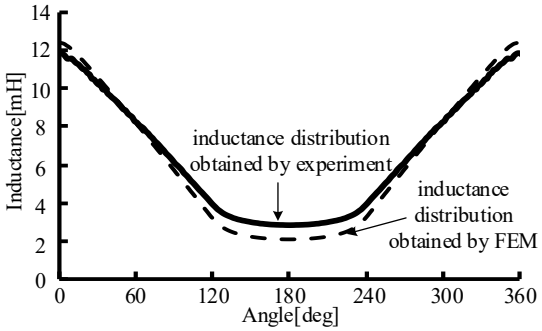

Fig. 7. Inductance profile obtained by the experiment and FEM analysis.

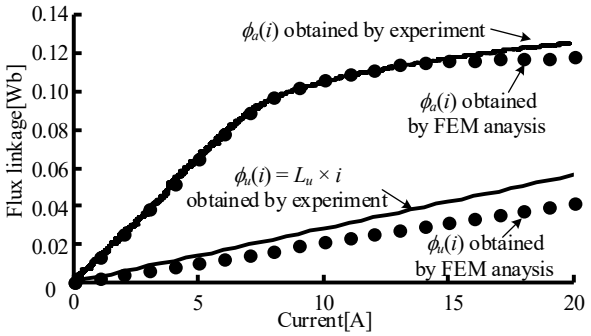

Fig. 8. i-ϕ characteristics obtained by the experiment and FEM analysis.

and the FEM analysis. The flux linkage at the aligned position is measured by applying the one-pulse voltage [15]. The flux linkage at the unaligned position is calculated from L_{un} in Fig. 7. The FEM analysis result have the error compared with the experimental result because FEM analysis cannot consider the effect of the flux leakage at the coil ends.

Experimental verification of torque ripple suppression method in linear region

Fig. 9 shows the current and the torque waveforms of (a) the conventional control with constant *dq*0-axis current and (b) the torque ripple suppression method using (11). The rotation speed is 235r/min and the current command I_q and I_0 is 4 A in this experiment. As shown in Fig. 9, the torque ripple is large when the conventional control is applied. On the other hand, the torque ripple is reduced by the proposed method.

Fig. 10 shows the harmonic analysis result of the torque waveforms in Fig. 9. As shown in Fig. 10, the torque ripple suppression method using (11) reduces the third-component of torque ripple by 76.1% compared to the conventional method with the constant *dq*0-axis current. In the linear region, the torque ripple is significantly reduced by the proposed method.

Experimental verification of average torque control in magnetic saturation region

Fig. 11 shows the average inductance L_{a_avg}, the incremental inductance L_{a_inc}, and the inductance L_{a_int} defined in this paper. L_{a_avg} and L_{a_inc} are smaller value than L_{a_int}. In other words, the area of the i-ϕ characteristic estimated from L_{a_avg} and L_{a_inc} estimate is smaller than that from L_{a_int}. Therefore, the calculated average torque from the L_{a_avg} and L_{a_inc} is smaller than the actual torque value in the magnetic saturation region.

Fig. 12 shows the comparison result of the average toque from the experimental value and from the torque equation. The rotation speed is 222 r/min and the current command is changed from 1A to 8A in this experiment. As shown in Fig. 12, the error occurs between the experimental result and the calculation result using the conventional equation. On the other hand, the calculation result using the derived equation almost agree with the experimental result with the error of 3.9%. The error of the proposed method are improved by 30.2pt compared to that of the conventional method. The average torque follows the command by using (15).

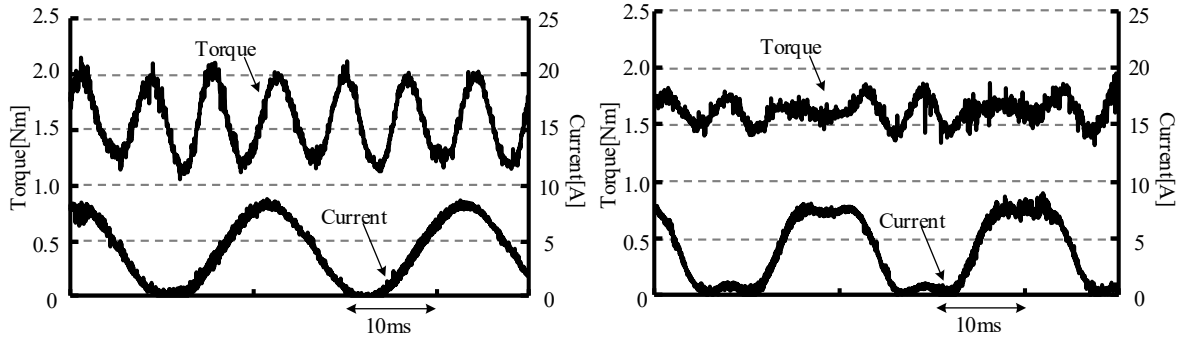

(a) Conventional method with the constant *dq*0 current.

(b) Torque ripple suppression method using (11).

Fig. 9. Experimental result in the linear region.

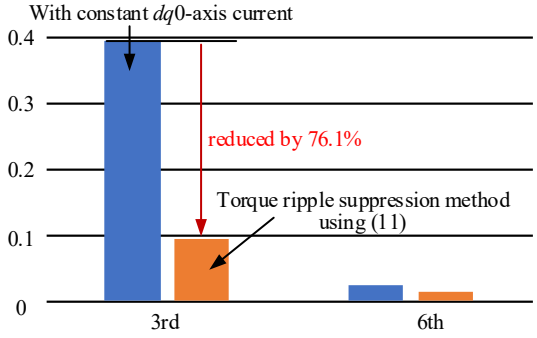

Fig. 10. Harmonic analysis result of the torque waveforms at $I_q = I_0 = 4$ A.

Experimental verification of torque ripple suppression method in magnetic saturation region

Fig. 13 shows the current and the torque waveforms for (a) the conventional control with the constant *dq*0-axis current, (b) the toque suppression method using (11), and (c) the torque ripple suppression method using (21). The rotation speed is 235r/min and the current command I_q, I_0 is 7A in this experiment. As shown in Fig. 13(b), the torque ripple is reduced by the toque ripple suppression method using (11) compared with that of the conventional control. However, the torque ripple remains due to the magnetic saturation. As shown in Fig. 13(c), the torque ripple is reduced by the torque ripple suppression method using (21) compared with that of the toque suppression method using (11).

Fig. 14 shows the harmonic analysis result of the torque waveforms in Fig. 13. As shown in Fig.14, the torque ripple suppression method using (11) reduces the third-order component of the torque ripple by 47.9% compared to the conventional method with the constant *dq*0-axis current. On the other hand, the torque ripple suppression method using (21) reduces the third-order component of the torque ripple by 73.4% compared to the conventional method with the constant *dq*0-axis current. From Fig. 13 and Fig. 14, the torque ripple is suppressed by the proposed method in the magnetic saturation region.

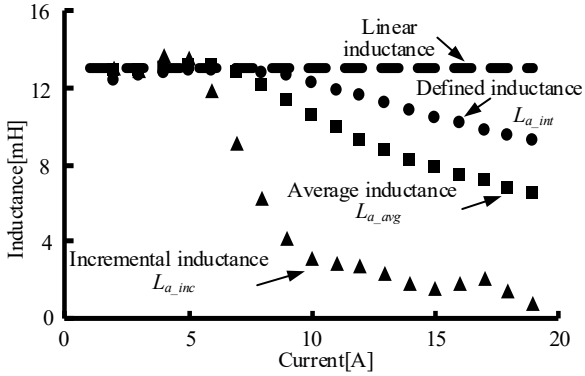

Fig. 11. Relationship between current and each inductance.

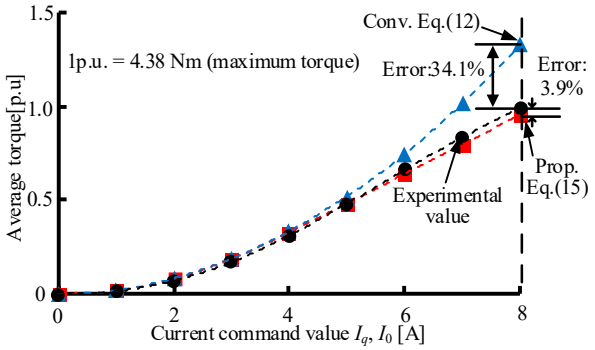

Fig. 12. Comparison of the average toque from experiment and torque equations.

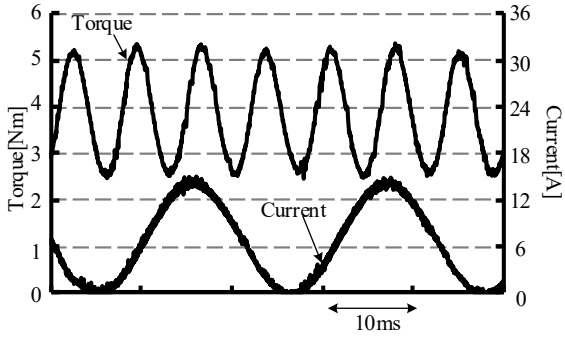

(a) Conventional method with the constant *dq*0 current.

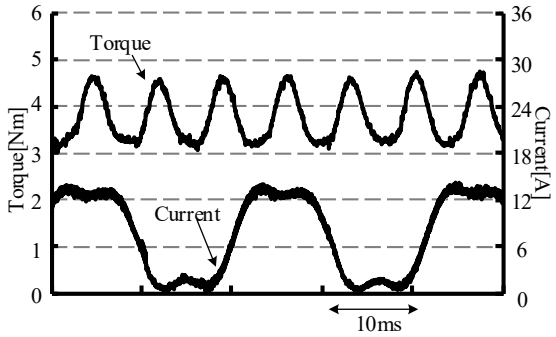

(b) Torque ripple suppression method using (11).

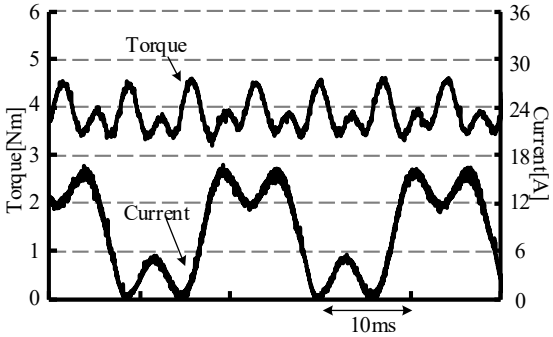

(c) Torque ripple suppression method using (21).

Fig. 13. Experimental results in the magnetic saturation region.

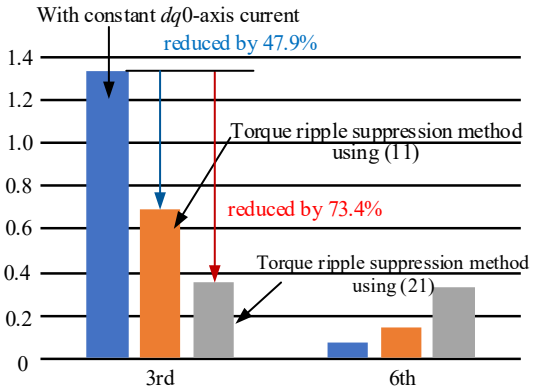

Fig. 14. Harmonic analysis result of the torque waveforms at $I_q = I_0 = 7$ A.

Conclusion

This paper proposed the torque ripple suppression method in the flux whole region without the FEM analysis. First, the third-order harmonic component of the zero-phase current was derived from the torque equation considering the spatial harmonics of the inductance profile in order to suppress the torque ripple. By applying the calculated zero-phase current command, the torque ripple was reduced by 76.1% compared with the conventional method using the constant $dq0$-axis current. Furthermore, this paper proposed the torque ripple suppression method in the magnetic saturation region. By applying the proposed method, the torque ripple was reduced by 73.4% compared with the conventional method using the constant $dq0$-axis current.

References

[1] S. Shin, H. Naruse, T. Kosaka and N. Matsui:“Torque Ripple Minimization Control in SRM Based on Magnetizing Curve Model Considering Mutual Coupling”, IEEJ Journal of Industry Applications, Vol.9, No.6, pp.637-649 (2020)

[2] Y. Ishihara, M. Sugiura, H. Ishikawa and H. Naitoh:“Improving the Efficiency of Switched Reluctance Motors using a Step-Skewed Rotor”, IEEJ Journal of Industry Applications, Vol.4, No.4, pp.445-453 (2015)

[3] N. Tashiro, K. Nakamura:“A Novel Control Method for In-wheel SR Motor to Implement Torque Vectoring Control for Compact EV” IEEJ Journal of Industry Applications, advance publication (2021)

[4] S. Samaka: “Fast Analytical Model for Switched Reluctance Machines” IEEJ Journal of Industry Applications, Vol.4, No.4, pp.352-359 (2015)

[5] Miller T. J. E.: Electronic Control of Switched Reluctance Machines, pp.74-97 (2001)

[6] J. Furqani, M. Kawa, K. Kiyota and A. Chiba:“Current Waveform for Noise Reduction of a Switched Reluctance Motor under Magnetically Saturated Condition”, IEEE Transactions on Industrial Application, Vol.54, No.1, pp.213-222 (2018)

[7] J. Furqani, M. Kawa, C. A. Wiguna, N. Kawata, K. Kiyota and A. Chiba:“Current Reference Selection for Acoustic Noise Reduction in Two Switched Reluctance Motors by Flattening Radial Force Sum” , IEEE Transactions on Industrial Application, Vol. 55, no. 4, pp. 3617-3629 (2019)

[8] H. Li, B. Bilgin and A. Emadi:“An Improved Torque Sharing Function for Torque Ripple Reduction in Switched Reluctance Machines”, IEEE Transactions on Industrial Application, Vol. 34, no. 2, pp.1635-1644 (2019)

[9] J. Ye, B. Bilgin and A. Emadi: “An Offline Torque Sharing Function for Torque Ripple Reduction in Switched Reluctance Motor Drives”, IEEE Transactions on Energy Conversion, Vol. 30, no. 2, pp. 726-735 (2015)

[10] J. Kim and J. Lai:“Quad Sampling Incremental Inductance Measurement Through Current Loop for Switched Reluctance Motor”, IEEE Transactions on Instrumentation and Measurement, Vol. 69, no. 7, pp. 4251-4257 (2020)

[11] V. Rallabandi, S. Mallampalli, R. Rahul and D. A. Torrey:“Performance Comparison of Switched Reluctance Motor with Sinusoidal and Conventional Excitation”, IEEE Energy Conversion Congress and Exposition (ECCE), pp.5580-5585 (2015)

[12] N. Nakao and K. Akatsu:“Vector control specialized for switched reluctance motor drives”, International Conference on Electrical Machines (ICEM), pp.943-949 (2014)

[13] N. Nakao and K. Akatsu:“Vector control for switched reluctance motor drives using an improved current controller”, IEEE Energy Conversion Congress and Exposition (ECCE), pp.1379-1386 (2014)

[14] K. Hu, Y. Chen and C. Liaw:“A Reversible Position Sensorless Controlled Switched-Reluctance Motor Drive With Adaptive and Intuitive Commutation Tunings”, IEEE Transactions on Power Electronics, vol. 30, no. 7, pp. 3781-3793 (2015)

[15] K. Kiyota, T. Kakishima, H. Sugimoto and A. Chiba:“Comparison of the Test Result and 3D-FEM Analysis at the Knee Point of a 60 kW SRM for a HEV”, IEEE Transactions on Magnetics, vol. 49, no. 5, pp. 2291-2294 (2013)